Mining Macroseismic Fields to Estimate the Probability Distribution of the Intensity at Site

G. Zonno   R. Rotondi *   C. Brambilla

Abstract

The analysis of the seismic attenuation is a prominent and problematic component of hazard assessment. Over the last decade it has become increasingly clear that the intrinsic uncertainty of the decay process must be expressed in probabilistic terms. This implies estimating the probability distribution of the intensity at a site I_s as the combination of the distribution of the decay ΔI and of the distribution of the intensity I_0 found for the area surrounding that site. We focus here on the estimation of the distribution of ΔI. Previous studies presented in the literature show that the intensity decay in Italian territory varies greatly from one region to another, and depends on many factors, some of them not easily measurable. Assuming that the decay shows a similar behavior in function of the epicenter-site distance when the same geophysical conditions and building vulnerability characterize different macroseismic fields, we have classified some macroseismic fields drawn from the Italian felt report database by applying a clustering algorithm. Earthquakes in the same class constitute the input of a two-step procedure for the Bayesian estimation of the probability distribution of ΔI at any distance from the epicenter, conditioned on I_0, where ΔI is considered an integer, random variable, following a binomial distribution. The scenario generated by a future earthquake is forecast either by the predictive distribution in each distance bin, or by a binomial distribution whose parameter is a continuous function of the distance. The estimated distributions have been applied to forecast the scenario actually produced by the Colfiorito earthquake on 1997/09/26; for both options the expected and observed intensities have been compared on the basis of some validation criteria. The same procedure has been repeated using the probability distribution of ΔI estimated on the basis of each class of macroseismic fields identified by the clustering algorithm.

1   Introduction

Most of the relationships proposed in the literature as models of seismic intensity attenuation come either from a physically consistent approach to the problem or from empirical analysis of the increase in intensity decay as the distance between epicenter and site increases. The former includes the papers by Gupta and Nuttli (1976) and by Von Kovesligethy (1906), which correlate the intensity with the ratio between the amplitude and the period of the seismic waves, and with the maximum acceleration, respectively. The latter examines the functional relations between intensity decay and distance deduced from the empirical evidence: the logarithm (Grandori *et*

---

*Corresponding author: `reni@mi.imati.cnr.it`

al., 1987), the square and cubic root (Berardi *et al.*, 1993), and the bilinear model (Gasperini, 2001) are the most frequently applied functions. The qualitative nature of the intensity and the influence of source and site responses on the decay process cause a huge dispersion of the observations. This uncertainty is generally dealt with by including in the model a gaussian error centered on the value of the above relationships with an assigned standard deviation.

As we think that the stochastic nature of the variable ΔI must be exploited from the start in assigning the intensity attenuation, we invert the usual manner of approach: we make no assumption regarding the functional relation between intensity decay and distance, but let the observations determine specific probability distributions for the random variables of the process, according to the local characteristics of the seismic energy propagation. Recent studies of all of Italy (Carletti and Gasperini, 2003) have shown the strong variability of the attenuation properties from one region to another. We consequently employ a hierarchical clustering algorithm to initially decompose a set of macroseismic fields representative of the temporal and spatial distribution of seismicity in Italy in order to select subsets of fields that are homogeneous from the viewpoint of attenuation. As the difference in trends depends on many geological characteristics, some of them not available nor easily measured (focal depth, heat flow, topographical and geological characteristics of the site), we apply a clustering procedure to the location and dispersion measures computed for each set of epicenter-site distances for which the same intensity was recorded. In Section 2.1 we describe the hierarchical agglomerative clustering method employed.

In this way we identify three classes $\mathcal{C}_{\mathbf{A}}, \mathcal{C}_{\mathbf{B}}, \mathcal{C}_{\mathbf{C}}$ of macroseismic fields of decreasing attenuation. To each of these classes we have applied the probabilistic analysis presented in Rotondi and Zonno (2004) to estimate the probability distribution of the intensity at a site conditioned on I_0 and the epicenter-site distance (Section 2.2). The analysis is performed within a Bayesian framework, which allows us to exploit different sources of information. Assuming, for instance, that the epicentral intensity is equal to the VIII degree of the Mercalli-Cancani-Sieberg (MCS) scale (Sieberg, 1931) and that we are considering class $\mathcal{C}_{\mathbf{A}}$, we can draw prior information on the model parameters from the macroseismic fields in this class with $I_0 \neq VIII$. We then update the parameters, considering fields of the same class, but with $I_0 = VIII$. To respect as much as possible the ordinal nature of the intensity variable, we have chosen as its probability distribution a discrete, binomial distribution on $[0, I_0]$ whose parameter p is considered a beta distributed random variable according to the Bayesian approach. Because the attenuation depends on the epicenter-site distance, the data are subdivided in distance bins around the epicenter, and the different distributions estimated for each bin.

In this way the posterior distribution of the p parameter summarizes the knowledge contained in the data set. Before a new observation is recorded, the expected likelihood with respect to the posterior distribution of p expresses the uncertainty regarding its value; this function is called the predictive distribution. In Section 2.3 it has been computed for the case of the binomial-beta model, obtaining the probability distribution of the future felt intensity in each distance bin, given I_0. Moreover, by smoothing the posterior means of p in each bin, we express the parameter as a function of the distance considered as a continuous variable. The binomial distribution in which the parameter is given by this function can be used instead of the predictive distribution

to predict the site intensity at any distance from the epicenter. To test these clustering and estimation procedures we have forecast the scenario actually observed in the Italian Colfiorito earthquake of 26 September 1997 (Section 3). This event is of course subsequent to those forming the data set used to define the procedure just outlined. For both the predictive and the smoothed binomial distributions the forecasting is given in terms of mode, probability of exceeding a given intensity, and value of I_s not exceeded with at least a fixed probability value. The scenarios estimated for each of the three classes $\mathcal{C}_{\mathbf{A}}$, $\mathcal{C}_{\mathbf{B}}$, $\mathcal{C}_{\mathbf{C}}$ are compared through three different validation criteria. Some remarks and the still unresolved issues indicated in Section 4 conclude the paper.

2 From macroseismic fields to intensity at site through probability distributions

The logical route we have covered to arrive at the characterization of the intensity at a site in terms of probability distribution starting from macroseismic fields can be described by listing the issues (I) that we have encountered and the solutions (A) that we have proposed.

Issue 1. Reducing the complexity of the data set?

In order to examine the macroseismic fields of a set of earthquakes representative of the spatial distribution of seismicity in Italy, we chose the 55 earthquakes with good quality macroseismic data sets already studied in Cella et al. (1996) and Peruzza (1996). They cover the period between 1560 and 1980 and are of an intensity between the VII and XI degree of the MCS scale. Their epicentral location is shown in Figure 1, while Table 1 provides the date, epicentral coordinates, epicentral macroseismic intensity, and number of felt reports for each earthquake. The corresponding macroseismic fields have been taken from the DBMI04 Italian database (see Data and Resources Section), considering only the intensity points for which numerical values were available; we have neglected the codes used for classifying effects not assessable in terms of macroseismic intensity like environment effects (EE), information coming from single buidings (SB) or small settlements (SS), and effects concerning an extended territory (TE) (Stucchi et al. (2007)). In this way we have formed a large data set with thousands of observations.

Table 1 and Figure 1 about here

Figure 2 is a graphic representation of some macroseismic fields chosen from the data set to show the different decay trends we saw when the same descriptive analysis was performed on the entire data set. The red dots mark the intensity decay *versus* the epicenter-site distance; the blue dots are the median values of distances of the same ΔI. The problem then was to find the way of summarizing the data and quantifying their basic features, that is, how to extract the implicit, hidden information from the data in order to identify meaningful patterns.

Figure 2 about here

Sets of observations are commonly summarized through measures of *location* (or *central tendency*) such as the arithmetic mean, the median, or the mode, and measures of *dispersion* or *variability*, such as the standard deviation, or the interquartile range. We have expressed every macroseismic field of the data set as a $3 \times I_0$ matrix (see, for example, Table 2), by evaluating the median, mean, and 3rd quartile of each set of epicenter-site distances with the same ΔI. The data in Table 2 are incomplete because $\Delta I = I_0 - 1 = 6$ was not recorded in any site.

Table 2 about here

Issue 2. Identifying similar behaviors

Then, setting the rows of each of the 55 tables in a single line, we collected the entire data set together in a $(55 \times 3\ I_0)$ matrix. In this way we passed from thousands of observations to less than 1500 data which still preserve most of the information contained in the original 55 macroseismic fields. As we have observed above, the attenuation trend of some of these fields seem similar, but how and on what basis can the "similar" ones be recognized?

Answer 2. Clustering techniques

The object is to form groups such that elements in the same group are similar to each other, whereas those in different groups are as dissimilar as possible. Following the terminology of cluster analysis we have $n = 55$ objects to be clustered, each of them represented by $p = 3\ I_0$ attributes, which we have arranged in an n-by-p matrix $\mathcal{X}$. The next step consists in computing the distance between each pair of objects i and j in order to quantify their degree of dissimilarity. The most popular choices are the *Euclidean distance* and the *city block* or *Manhattan distance*, defined respectively by:

$$d(i,j) = \sqrt{(x_{i1} - x_{j1})^2 + (x_{i2} - x_{j2})^2 + \ldots + (x_{ip} - x_{jp})^2}$$

and

$$d(i,j) = \mid x_{i1} - x_{j1} \mid + \mid x_{i2} - x_{j2} \mid + \ldots + \mid x_{ip} - x_{jp} \mid \tag{1}$$

where $(x_{i1}, x_{i2}, \ldots, x_{ip})$ and $(x_{j1}, x_{j2}, \ldots, x_{jp})$ are the attributes of the two objects, each a row of the $\mathcal{X}$ data matrix. We have preferred the Manhattan distance (1) because it is not particularly sensitive to outliers in the sense that a single outlying measurement will not have an exaggerated influence on $d(i,j)$. We have evaluated the resulting n by n matrix $\mathcal{D}$ of dissimilarities by applying the subroutine DAISY of the S-Plus library, version 6.2.1. (S-Plus, 2003). This is a symmetric matrix and therefore we need to store only its lower triangular half. As already

noted in Table 2 not all the measurements may actually be available. In these cases, if ng is the number of the columns of $\mathcal{X}$ in which neither row i nor j have missing data, then the dissimilarity returned by the algorithm is p/ng times the dissimilarity $d(i,j)$ (1) between the two vectors of length ng shortened to exclude the missing values.

The matrix thus obtained can now be used as the input data structure of clustering algorithms, either partitioning or hierarchical. The former divide tha data set into k clusters, where the interger k must be specified, whereas the latter deal with all values of k in the same run. Since the identification of the number k of different attenuation trends is one of the objectives of our analysis, we have used a *hierachical agglomerative* algorithm (Kaufman and Rousseeuw, 1990) implemented by the AGNES routine of the S-PLUS library.

2.1 Building classes of macroseismic fields

In agglomerative clustering methods each object is initially considered as a separate cluster: at step 0 one has n clusters, in the first step the two objects with the least dissimilarity are joined in a cluster, and in all the successive steps the two closest clusters are merged until only one cluster is left. Agglomerative algorithms are characterized by the definition of between-cluster dissimilarity. According to the *complete linkage* (or *furthest neighbour*) method the dissimilarity between two clusters R, Q is defined as the greatest dissimilarity between an object i of the one cluster and an object j of the other cluster, that is

$$d(R,Q) = \max_{i \in R,\ j \in Q} d(i,j) \qquad .$$

In the *single linkage* (or *nearest neighbour*) method the dissimilarity is given by the least dissimilarity between an object i of R and an object j of Q:

$$d(R,Q) = \min_{i \in R,\ j \in Q} d(i,j) \qquad .$$

The difference between these inter-cluster distances is highlighted by the bidimensional representation ($p = 2$) of the resulting groups. The single-linkage method tends to form elongated clusters where some members may be very far from each other. This property, called the *chaining effect*, is an advantage in some applications, but in general renders the method undesirable because poorly separated clusters are linked together. The opposite holds for the complete linkage method which tends to produce very compact clusters of strongly similar objects with the disadvantage that relatively similar objects may remain in different clusters for many cycles of the clustering algorithm. For this reason complete linkage is said to be *space dilating*. To mediate between these two extremes other *space conserving* inter-cluster distances have been proposed by Späth (1980), Anderberg (1973), and in particular Ward (1963), who devised a procedure to partition a set so as to minimize the loss of information associated with each grouping: let $\bar{x}_R$ denote the centroid of the cluster R, defined by $\bar{x}_k = 1/m_R \sum_{i \in R} x_{ik}$, $k = 1, \ldots, p$, that is, the point in the p-dimensional space whose coordinates are the arithmetic mean of the attributes of the m_R objects in the cluster R. Ward defined the information loss associated with this cluster in terms of the error sum of centroid-object distances

$$E_R = \sum_{i \in R} d(x_i, \bar{x}_R) \qquad .$$

At each step the union of every possible pair of clusters R, Q, generating a new cluster T, is considered, and the two clusters whose merger results in the minimum increase ΔE in information loss are combined; hence ΔE is given by

$$\Delta E = \min_{R,Q} \Delta E_{RQ} = E_T - E_R - E_Q \qquad .$$

In varying the between-object and between-cluster dissimilarities, the user is faced with a multitude of methods to choose from. Some quantitative and graphic measures of the clustering structure can be used to this end: the *agglomerative coefficient AC*, the *overall average silhouette width* and its plot (Rousseeuw, 1987), the *dendrogram* or cluster tree (Kaufman and Rousseeuw, 1990).

The hierarchy produced by the AGNES algorithm is well displayed graphically as a tree in which the leaves represent the objects, while the vertical coordinates of the junction of two branches are the dissimilarities between the corresponding clusters (Struyf *et al.*, 1996). An example of this agglomerative tree, which we will discuss later, is given in Figure 3.

Figure 3 about here

For each object i, $i = 1, \ldots, n$, let us denote by $l(i)$ its dissimilarity to the first cluster it is merged with, divided by the dissimilarity of the merger in the final step of the algorithm. The AC is the average of all $(1 - l(i))$, a value between 0 and 1 which describes the strength of the clustering structure obtained by the clustering algorithm. The higher the AC value, the clearer the clustering structure.

The silhouette value $s(i)$ of each object is computed as follows: let A be the cluster to which object i belongs and $a(i)$ the average dissimilarity of i to all other objects in A. Then let us consider any cluster C different from A and let $d(i, C)$ be the average dissimilarity of i to all objects of C. After identifying the cluster B such that

$$b(i) = d(i, B) = min_{C \neq A} d(i, C) \qquad ,$$

we define $s(i)$:

$$s(i) = \frac{b(i) - a(i)}{max\left\{a(i), b(i)\right\}} \qquad .$$

B is the *neighbor* of object i and the second-best cluster for object i. The value $s(i)$ always lies between -1 and +1, and it is clear that if $s(i) \approx 1$, object i is well classified, whereas if $s(i) \approx -1$, object i is badly classified. The *overall average silhouette width* is then defined as the average of the $s(i)$ over all objects i in the data set. The graphic representation of this quality index is a plot showing the silhouettes of all clusters next to each other, where the silhouette of a cluster is a plot of the $s(i)$, ranked in decreasing order, of all its objects i. The subroutine CUTREE of the S-PLUS library provides a division of the tree produced by AGNES into a fixed number k of groups (Venables and Ripley, 2002): climbing the tree in Figure 3 and cutting in turn the branches at the junctions with the highest dissimilarity, at the fourth cut we have $k = 5$ well-separated groups, the three differently coloured and the two single earthquakes of 1875/12/06

and 1743/02/20. The corresponding silhouette plot, produced by the R free software (R Development Core Team, (2008)), is given in Figure 4 (*top*) with an average silhouette width of 0.26.

Figure 4 about here

Let us go back to the tree in Figure 3. It is obtained with the Manhattan metric and Ward's method, and its agglomerative coefficient is $AC = 0.9517$. We have also considered other hierarchical agglomerative methods: single-, complete-, average-linkage, and the `Euclidean` metric. We decided on the Manhattan-Ward combination for its quality indices and the sharpness of the clustering structure. In fact the largest agglomerative coefficient, $AC = 0.9544$, associated with the Manhattan-complete linkage combination, is just little higher than the second best value, $AC = 0.9517$, of the Manhattan-Ward combination, whereas the clustering structure produced through Ward's method and indicated by the silhouette plot in Figure 4 (*top*) shows a clearer and more homogeneous partition of the data than that of the silhouette plot generated by the complete-linkage method (Figure 4, *bottom*). Consequently, we consider the data set to be formed mainly by three classes. The isolated earthquakes 1875/12/06 and 1743/02/20 are considered to have an atypical, not generalizable behavior and therefore are not classified.

Now we must see if the clustering technique applied has been able to answer Issue 2 or, in other words, if the classes identified are really characterized by similar attenuation trends. To do so we reorganize Figure 2 ordering the macroseismic fields according to the classification just found. The result is shown in Figure 5. The **A** column, on the left, contains the fields of the earthquakes with the steepest attenuation trend, indicated in yellow in Figure 3. The **B** column, in the middle, corresponds to the earthquakes with a less steep trend, red in Figure 3. The **C** column on the right gathers fields presenting a flatter attenuation trend, violet in Figure 3. Comparing the different trends from left to right we may conclude that the result of the clustering process is visually consistent. Figure 6 shows the spatial distribution of the resulting three classes of attenuation.

Figures 5 and 6 about here

2.2 Probabilistic model

Having grouped the set of macroseismic fields in homogeneous classes we can now address the problem of attenuation modelling in the strict sense. First of all we must consider the nature of the intensity decay ΔI. It is a variable affected by intrinsic uncertainty that is expressed suitably through an additional Gaussian error; for instance, Figure 7 represents the relative frequencies of the decay recorded in distance bins 10 km wide around the epicenter of the 1980 Irpinia-Basilicata earthquake, a shock of $I_0 = X$ with a rich macroseismic field of 1161 data points from $\Delta I = 0$ to $\Delta I = VII$. We note that as we move away from the epicenter, the empirical probability function of ΔI runs along the domain $\{0, 9\}$, taking different shapes.

Figure 7 about here

Hence the intensity decay ΔI, like the macroseismic intensity, must to be treated as a random variable. As the variable ΔI is discrete and belongs to the domain $\{0, I_0 - 1\}$ it is reasonable to choose for $I_s = I_0 - \Delta I$, *at a fixed distance*, the binomial distribution $Bin(i_s|I_0, p)$ conditioned on I_0 and p:

$$
\begin{aligned}
Pr\left\{I_s = i \mid I_0 = i_0, p\right\} &= Pr\left\{\Delta I = I_0 - i \mid I_0 = i_0, p\right\} \\
&= \binom{i_0}{i} p^i (1-p)^{i_0 - i} \qquad i \in \{0, 1, \ldots, i_0\} \qquad .
\end{aligned}
\tag{2}
$$

and then restrict the support to be $\{1, I_0\}$ by defining $Pr\left\{I_s = 1\right\} = Pr\left\{I_s \leq 1\right\}$. Moreover, since the ground shaking may differ even among sites located at the same distance, we consider p as a random variable which follows a Beta distribution:

$$
Be(p; \alpha, \beta) = \frac{\Gamma(\alpha + \beta)}{\Gamma(\alpha)\Gamma(\beta)} \int_0^p x^{\alpha-1} (1-x)^{\beta-1} dx \qquad .
\tag{3}
$$

To analyze the probability distribution of ΔI, or analogously of I_s, given the epicentral intensity I_0, we follow the approach described in detail in Rotondi and Zonno (2004), with a modification in particular in the way of assigning the parameters α and β of the prior distribution (3).

We let $n_{\mathbf{A}}$ be the number of macroseismic fields of the data set in the class $\mathcal{C}_{\mathbf{A}}$ and, among these, let $n_{\mathbf{A}i}$ and $n_{\mathbf{A}\_i}$ be those with epicentral intensity $I_0 = i$ and with any epicentral intensity except $I_0 = i$ respectively, $i = 7, \ldots, 11$, analogously for classes $\mathcal{C}_{\mathbf{B}}$ and $\mathcal{C}_{\mathbf{C}}$. Hence $n = \sum_{i=7}^{11}(n_{\mathbf{A}i} + n_{\mathbf{B}i} + n_{\mathbf{C}i}) = 53$ (as the two atypical fields were not classified). To extract information from the historical data in order to assign the prior distributions we first draw L distance bins around the epicenter of every macroseismic field and indicate by $N_j^{(k)}$ the number of observed intensities at the jth bin ($j = 1, \ldots, L$) of the kth earthquake ($k = 1, \ldots, n$), and by $N_j^{(k)}(I_0)$ the number of those data points with $I_s = I_0$, or the number of sites where the decay is null. For the sake of simplicity we consider an earthquake with $I_0 = 9$ classified in class $\mathcal{C}_{\mathbf{A}}$ and, to assign the prior distributions, extract the information from the macroseismic fields of the same class, but with $I_0 \neq 9$, by applying the following algorithm:

step 1. assign *a priori* value to the parameter $p_{j,0}$ of each bin, $j = 1, \ldots, L$; initialize $j = 0$:

(a) $j \leftarrow j + 1$,

(b) for each of the n_{A_9} macroseismic fields compute $N_j^{(k)}$ and $N_j^{(k)}(I_0)$, $k = 1, 2, \ldots, n_{A\_9}$, as defined above; if $N_j^{(k)}(I_0) \neq 0$, then set $p_{j,0}^{(k)} \approx \left(\frac{N_j^{(k)}(I_0)}{N_j^{(k)}}\right)^{1/I_0}$,

(c) calculate $N_j = \sum_{k=1}^{n_{A\_9}} N_j^{(k)}$, if $\exists k : N_j^{(k)}(I_0) \neq 0$ then set $p_{j,0} \approx \sum_{k=1}^{n_{A\_9}} p_{j,0}^{(k)} N_j^{(k)}/N_j$, otherwise go to (a);

N.B. When $N_j^{(k)}(I_0) = 0$, $p_{j,0}^{(k)}$ is not calculated. Moreover if $\forall k$, $N_j^{(k)}(I_0) = 0$, $p_{j,0}$ as well cannot be evaluated; hence $p_{j,0}$ is given only in those jth bins where $\exists k : N_j^{(k)}(I_0) \neq 0$. The

estimate of $p_{j,0}$ given in (c) is the combination of the estimates (relative frequencies (b)) $p_{j,0}^{(k)}$ produced through independent information sources.

step 2. Assign p_0 at any distance d:

(d) approximate the available $p_{j,0}$'s by an inverse power function $f(d) = (c_1/d)^{c_2}$ (*smoothing function*), and estimate the coefficients c_1, c_2 by the method of least squares,

(e) set, for each bin $j = 1, 2, \ldots, L$, $p_{j,0} = f(r_j - \Delta r/2)$ where r_j is the radius of the jth bin and Δr is the bin width,

(f) $p_{j,0}$ can be considered as the *a priori* mean of the variable p_j, the variance $\sigma^2(p_j)$ is assigned as suggested in Rotondi and Zonno (2004, Section 2.1), for instance, equal to the mean-square error of the approximating function $f(d)$.

step 3. By inverting the mean and variance of the Beta distribution (3)

$$E_0(p_j) = \frac{\alpha_{j,0}}{\alpha_{j,0} + \beta_{j,0}} \qquad \sigma^2(p_j) = \frac{\alpha_{j,0}\beta_{j,0}}{(\alpha_{j,0} + \beta_{j,0})^2(\alpha_{j,0} + \beta_{j,0} + 1)} \qquad (4)$$

obtain the prior hyperparameters $\alpha_{j,0}$, $\beta_{j,0}$, $j = 1, 2, \ldots, L$.

step 4. Update the hyperparameters $\alpha_{j,0}$, $\beta_{j,0}$:

(g) by means of the n_{A9} macroseismic fields of the class $\mathcal{C}_{\mathbf{A}}$ with $I_0 = 9$ or when a new earthquake of $I_0 = 9$ is recorded, update the estimate of p_j's through the posterior mean

$$\hat{p}_j = \frac{\alpha_{j,0} + \sum_{n=1}^{N_j} i_s^{(n)}}{\alpha_{j,0} + \beta_{j,0} + I_0 \cdot N_j} \qquad , \qquad (5)$$

(h) smooth the estimates $\hat{p}_j, j = 1, \ldots, L$ with the method of least squares, by using an inverse power function $g(d) = (\gamma_1/d)^{\gamma_2}$,

(i) by again inverting (4), obtain α_j and β_j, hyperparameters of the Beta distribution of p_j, for each bin $j = 1, 2, \ldots, L$.

N.B. the α_j's and β_j's really updated are only those associated with the bins where data points were observed.

The results of this procedure for the three classes $\mathcal{C}_A$, $\mathcal{C}_B$, $\mathcal{C}_C$ can be seen in Figure 8; the top row shows the *a priori* value of the parameters $p_{j,0}$ (blue dots) and the *smoothing* function $f(d) = (c_1/d)^{c_2}$ (see Section 2.2, step 2. (d)) (red dots). The bottom row shows the *posterior* estimates of p_j, $j = 1, \ldots, 250$ (blue dots), the approximating curve $g(d) = (\gamma_1/d)^{\gamma_2}$ (see Section 2.2, step 4. (h)) (red dots), and the 90% confidence interval (green bars) of the binomial distribution (2) for each p_j. The red curves in Figure 8 do not represent the attenuation trend, but the trend of the estimated parameter $\hat{p}$ of the binomial distribution (2) of I_s as the distance from the epicenter varies.

Figure 8 about here

2.3 Building future scenarios

After estimating the parameter the probabilistic model of I_s is now completely defined, and we can think of how to forecast future scenarios. So far we have discretized the space around the epicenter by dividing it in bins where the distribution of I_s depends on I_0 and on the parameter p_j, characteristic of the bin, hence the model is given by:

$$Pr\{I_s \mid I_0, p_j\} \times Pr\{p_j \mid I_0; \alpha_j, \beta_j\} \qquad .$$

To take into account the uncertainty on p_j we average the model over this random variable obtaining the *predictive* distribution:

$$Pr_{pred}\{I_s = i \mid I_0\} = \begin{pmatrix} i_0 \\ i \end{pmatrix} \frac{\Gamma(\alpha_j + \beta_j)}{\Gamma(\alpha_j)\Gamma(\beta_j)} \frac{\Gamma(\alpha_j + i)\Gamma(\beta_j + i_0 - i)}{\Gamma(\alpha_j + \beta_j + i_0)} \qquad , \qquad (6)$$

where α_j and β_j are those obtained in Section 2.2, step 4. (i). If, on the contrary, we want to have the distribution of I_s at any site at distance d from the epicenter, we may substitute p in the binomial distribution (2) by the value of the smoothing function $g(d)$ given in Section 2.2, step 4. (h). which approximates the posterior means of p_j's. In the following we shall indicate this binomial distribution as:

$$Pr_{smooth}\{I_s = i \mid I_0; g(d)\} = \begin{pmatrix} i_0 \\ i \end{pmatrix} g(d)^i (1 - g(d))^{i_0 - i} \qquad i \in \{0, 1, \ldots, i_0\} \qquad . \qquad (7)$$

Figure 9 shows, for each attenuation class of earthquakes of $I_0 = 9$, the predictive distribution (left) and the *smoothing* binomial distribution (right) of I_s in each bin. In particular, in the jth bin we took as the epicenter-site distance $d = r_j - \Delta r/2$, $j = 1, 2, \ldots, 160$. The predictive distributions are flatter than the binomials because of the averaging over the p's parameters performed to obtain (6).

Figure 9 about here

The mode of the above distributions, i_{pred} or i_{smooth}, can be used as the predicted value of the intensity at sites located inside the respective bins if we are using the predictive distribution (6), or at sites at distance d from the epicenter if we are using the binomial distribution (7) with parameter $g(d)$. Since $I_s = 0$ does not make sense, we suggest assigning $Pr(I_s \leq 1 \mid I_0)$ to $Pr\{I_s = 1 \mid I_0\}$ in hazard assessment.

3 A case study: the Colfiorito earthquake

The data set in Table 1 covers the period 1570-1980. After this date the strongest earthquake that occurred in Italy was the 1997 Colfiorito earthquake in the Umbria-Marche region. The seismic sequence began on 26 September 1997 with two main shocks: the first event, $M_L = 5.6$, occurred at 00:33 GMT, the second, $M_L = 5.8$, several hours later, at 09:40 GMT. A third quake, $M_L = 5.5$, occurred on 14 October at 15:33 GMT (Amato *et al.*, 1998). The epicenter

was located at Colfiorito Lon. 12.879E, Lat. 43.020N (Gasperini *et al.*, 1999), and the damage ascertained in the days immediately following the main shock has been associated with the IX degree of the MCS scale (ING *et al.*, 1997). Figure 10 (middle) shows the 362 felt reports recorded in a radius of 150 km from the epicenter, with intensities varying from the IX to the IV degree. The position of the epicenter with respect to the other earthquakes in the data set is indicated in Figure 6 by a black square. It is situated along the line which joins up two earthquakes of class $\mathcal{C}_A$ (yellow): the northernmost, the 1781/06/03 Cagliese earthquake of the IX-X degree, and the southernmost, the 1703/01/14 Reatino Apennines earthquake of the XI degree, but it is also near the 1741/04/24 Fabrianese earthquake of the IX degree listed in class $\mathcal{C}_C$.

Figure 10 about here

Let us consider each site of the Colfiorito macroseismic field where the intensity was assigned, and compute the two distributions of the intensity at site: the predictive distribution (6) according to the membership bin, and the binomial distribution (7) where d is the specific distance from the epicenter. We repeat the same procedure for each of the three classes of attenuation and estimate the intensity at sites through the mode of these distributions. Figure 11 represents the expected intensities or, in other words, the expected scenarios given the epicentral intensity IX, while the left and right pictures in Figure 10 show the discrepancy between observed and expected intensities obtained through the predictive and binomial distribution, respectively. The differences between the distributions of I_s noted at the end of Section 2.3 are reflected in Figure 11: in both families of distributions the attenuation globally decreases passing from the class $\mathcal{C}_A$ to the class $\mathcal{C}_C$ but, on the one side, the binomial distributions are more peaked so that higher intensities are estimated around the epicenter, while on the other side, the scenarios obtained by the predictive distributions may vary locally among the classes due to the irregular behavior of the estimated p_j's parameters (blue dots) in the *bottom* row of Figure 8. In fact higher intensities are estimated around the epicenter in class $\mathcal{C}_B$ while the trend again decreases monotonically far from the epicenter, going from $\mathcal{C}_A$ to $\mathcal{C}_C$.

Figure 11 about here

As result of the approach followed we have obtained not only estimates of the intensity at site, but also entire probability distributions of I_s (see Figure 9). We visualize this richness of information by representing in Figure 12 the probability that the felt intensity exceeds the VII degree of the MCS scale at the sites of the macroseismic field of the Colfiorito earthquake according to the different probability distributions of I_s proposed and the different attenuation classes. In the same conditions Figure 13 shows the intensity that is not exceeded with at least 70% of probability.

Figures 12 and 13 about here

To discriminate among the various forecast scenarios we compare the predicted values with

those observed, applying the validation criteria proposed in Lindley (1987) and Winkler (1996). We let N_j be the number of the felt reports in the jth bin, $j = 1, 2, \ldots, L$, and $N = \sum_{j=1}^{L} N_j$ be their total number. The set of $i_s^{(n)}$ intensity points per bin is indicated by $\mathcal{D}_j$ while $\mathcal{D} = \sum_{j=1}^{L} \mathcal{D}_j$ denotes the total data set. We measure the degree to which each model predicts the data by the *logarithmic scoring rule*, a probabilistic measure based on the logarithm of a posterior probability, in our case the predictive (also called the *marginal likelihood*) and the binomial distributions (Rotondi and Zonno, 2004). We obtain respectively the following expressions:

$$score_{pred} = -\frac{1}{N} \log \prod_{j=1}^{L} \prod_{\substack{n = 1, \ldots, N \\ i_s^{(n)} \in \mathcal{D}_j}} \binom{I_0}{i_s^{(n)}} \frac{\Gamma(\alpha_j + \beta_j)}{\Gamma(\alpha_j)\,\Gamma(\beta_j)} \frac{\Gamma(\alpha_j + i_s^{(n)})\,\Gamma(\beta_j + I_0 - i_s^{(n)})}{\Gamma(\alpha_j + \beta_j + i_0)} \quad (8)$$

and

$$score_{bin} = -\frac{1}{N} \log \prod_{n=1}^{N} \binom{I_0}{i_s^{(n)}} g(d_n)^{i_s^{(n)}} \, (1 - g(d_n))^{(I_0 - i_s^{(n)})} \quad (9)$$

d_n being the distance of the $n-$th site from the epicenter. Another probabilistic measure of the fit is given by the $p(A)/p(B)$ ratio between the probability that the fitted model assigns to the realization A and the probability of the predicted value B; it is a measure of how much is gained from having predicted B when A occurs. The errors, expressed in probabilistic terms, are given by the geometric means of the corresponding *odds* in logarithmic scale:

$$odds_{pred} = -\frac{1}{N} \log \prod_{n=1}^{N} \frac{Pr_{pred}(i_s^{(n)} \,|\, \mathcal{D}_j)}{Pr_{pred}(i_{pred}^{(n)} \,|\, \mathcal{D}_j)} \quad (10)$$

$$odds_{bin} = -\frac{1}{N} \log \prod_{n=1}^{N} \frac{Pr_{smooth}(i_s^{(n)} \,|\, \mathcal{D})}{Pr_{smooth}(i_{smooth}^{(n)} \,|\, \mathcal{D})} \quad . \quad (11)$$

where $i_{pred}^{(n)}$ and $i_{smooth}^{(n)}$ are respectively the mode of the predictive and of the *smoothing* binomial distribution at the $n-$th site, estimator of the intensity at site (see Section 2.3).

Finally, we also apply a deterministic measure: the absolute discrepancy between observed and estimated intensities at site. It is given for the predictive and binomial distribution respectively by:

$$diff_{pred} = 1/N \sum_{n=1}^{N} \left| i_s^{(n)} - i_{pred}^{(n)} \right| \quad \text{and} \quad diff_{smooth} = 1/N \sum_{n=1}^{N} \left| i_s^{(n)} - i_{smooth}^{(n)} \right| \quad . \quad (12)$$

The results are reported in Table 3; the values denoted by * are the minima - the best values - of the different criteria over the attenuation classes, while ** indicates the minimum of the corresponding criterion when both the class and the distribution vary. For instance, according to the scoring rule the best value is obtained by forecasting the scenario through the predictive distribution of class $\mathcal{C}_A$, but the best score is provided by the same class using the binomial distribution as well. Apart from the absolute discrepancy between the intensities observed and those estimated by the binomial distribution, all the criteria support the conclusion that the

12

Colfiorito earthquake should be included in class $\mathcal{C}_A$.

Table 3 about here

4   Comments

We have followed an itinerary which has led us from a sufficiently large data set of macroseismic fields of the Italian territory to the forecasting of seismic scenarios in terms of macroseismic intensity. The first leg was the identification, through a clustering technique, of three different trends of attenuation, and hence the subdivision of the earthquakes into three classes. We have then analyzed a probabilistic model for the intensity decay, and through a Bayesian methodology estimated the probability distributions of the intensity at site I_s (or equivalently the decay ΔI) for bins, or at any distance from the epicenter. This methodology has been applied to forecast the seismic scenario of the Colfiorito 1997 earthquake without knowing the attenuation class to which it belongs. Comparison of the estimated intensities at site with those observed shows that this earthquake should be included in class $\mathcal{C}_A$ which, being characterized by the quickest attenuation, can be related to events of little depth. As a matter of fact, according to Cattaneo *et al.* (2000) the sequence of Colfiorito lasted until April 1998 and was characterized by shallow earthquakes, less than 9 km deep. Our analysis agrees perfectly with this. This preliminary result seems to support the idea that in Italy it would be better to regionalize the attenuation probabilistic laws instead of considering a national one, and that data-driven techniques should be used to divide the territory into isoattenuation zones rather than apply other criteria which have not been proved to be strongly correlated with intensity attenuation.

Data and Resources

The maps were produced using the Generic Mapping Tools (GMT) package by Wessel and Smith (www.soest.hawaii.edu/gmt, last accessed May 2009). The macroseismic fields of the DBMI04 Italian database were obtained from www.emidius.mi.ingv.it/DBMI04 (last accessed May 2009).

Acknowledgments

References

Amato, A., R. Azzara, C. Chiarabba, G. B. Cimini, M. Cocco, M. Di Bona, L. Margheriti, S. Mazza, F. Mele, G. Selvaggi, A. Basili, E. Boschi, F. Courboulex, A. Deschamps, S. Gaffet,

G. Bittarelli, L. Chiaraluce, D. Piccinini, and M. Ripepe (1998). The 1997 Umbria-Marche, Italy, earthquake sequence: a first look at the main shocks and aftershocks, *Geophys. Res. Lett.*, **25**, 15, 2861–2864.

Anderberg, M. R. (1973). *Cluster Analysis for Applications*, Academic Press, New York.

Berardi, R., C. Petrungara, L. Zonetti, L. Magri, and M. Mucciarelli (1993). *Mappe di Sismicità per l'Area Italiana*, ISMES, Bergamo, Italy, pp. 52.

Carletti, F., and P. Gasperini (2003). Lateral variations of seismic attenuation in Italy, *Geophys. J. Int.*, **155**, 839–856.

Cattaneo, M., P. Augliera, G. De Luca, A. Gorini, A. Govoni, S. Marcucci, A. Michelini, G. Monachesi, D. Spallarossa, L. Trojani, & XGUMS (2000). The 1997 Umbria-Marche (Italy) earthquake sequence: analysis of the data recorded by the local and temporary networks, *J. Seism.*, **4**, 4, 410–414.

Cella, F., G. Zonno, and F. Meroni (1996). Parameters estimation of intensity decay relationships, *Annali di Geofisica*, **39**, 5, 1095–1113.

Gasperini, P., F. Bernardini, G. Valensise, and E. Boschi (1999). Defining seismogenic sources from historical earthquake felt reports, *Bull. Seismol. Soc. Amer.*, **89**, 1, 94–110.

Gasperini, P. (2001). The attenuation of seismic intensity in Italy: a bilinear shape indicates the dominance of deep phases at epicentral distances longer than 45 km., *Bull. Seism. Soc. Am.*, **91**, 4, 826–841.

Grandori, G., F. Perotti, and A. Tagliani (1987). On the attenuation of macroseismic intensity with epicentral distance, In: *Ground Motion and Engineering Seismology*, A.S. Cakmak (editor), Elsevier, Amsterdam, 581-594.

Gupta, I.N., and O.W. Nuttli (1976). Spatial attenuation of intensities for central U.S. earthquakes, *Bull. Seism. Soc. Am.*, **66**, 3, 743–751.

ING, GNDT and SSN (1997). *Macroseismic survey after the earthquakes of 26 September 1997 and following days* updated on October 10, 1997, available from

http://emidius.mi.ingv.it/GNDT/T19970926

Kaufman, L., and P.J. Rousseeuw (1990). *Finding Groups in Data An introduction to cluster analysis*, Wiley & Sons, New York.

Lindley, D.V. (1987). The probability approach to the treatment of uncertainty in artificial intelligence and expert systems, *Statistical Science*, **2**, 17–24.

Peruzza, L. (1996). Attenuating intensities, *Annali di Geofisica*, **39**, 5, 1079–1093.

R Development Core Team (2008). *R: A language and environment for statistical computing*, R Foundation for Statistical Computing, Vienna, Austria. ISBN 3-900051-07-0, URL http://www.R-project.org

Rotondi, R., and G. Zonno (2004). Bayesian analysis of a probability distribution for local intensity attenuation, *Annals of Geophysics*, **47**, 5, 1521–1540.

Rousseeuw, P.J. (1987). Silhouttes: A graphical aid to the interpretation and validation of cluster analysis, *J. Comput. Appl. Math.*, 20, 53–65.

Späth, H. (1980). *Cluster Analysis Algorithms for data reduction and classification of objects*, Ellis Horwood Limited, Chichester.

S-Plus (2007). Insightful Corp. Version 8.0.4 for Linux 2.4.21

Sieberg, A. (1931). Erdebeben, in *Handbuch der Geophysic*, B. Gutenberg (Editor) Vol. 4, 552–554.

Struyf, A., M. Hubert, and P.J. Rousseeuw (1996). Integrating robust clustering techniques in S-Plus, *Computational Statistics & Data Analysis*, 26, 17–37.

Stucchi M., Camassi R., Rovida A., Locati M., Ercolani E., Meletti C., Migliavacca P., Bernardini F. and Azzaro R. (2007). DBMI04, il database delle osservazioni macrosismiche dei terremoti italiani utilizzate per la compilazione del catalogo parametrico CPTI04, *Quaderni di Geofisica*, **49**, pp.38.

Venables, W.N., and B.D. Ripley (2002). *Modern Applied Statistics with S*, Springer-Verlag, New York.

Von Kovesligethy, R. (1906). Seismonomia, *Boll. Soc. Sism. Ital.*, **XIV**.

Ward, J.H. (1963). Hierarchical grouping to optimize an objective function, *J. Am. Stat. Ass.*, **58**, 236–244.

Winkler, R.L. (1996). Scoring rules and the evaluation of probabilities, *Test*, **5**, 1, 1–60.

Gaetano Zonno

Istituto Nazionale di Geofisica e Vulcanologia, Sezione di Milano-Pavia

Via Bassini 15, 20133 Milano, Italy

zonno@mi.ingv.it

Renata Rotondi

C.N.R. - Istituto di Matematica Applicata e Tecnologie Informatiche

Via Bassini 15, 20133 Milano, Italy

reni@mi.imati.cnr.it

Carla Brambilla

C.N.R. - Istituto di Matematica Applicata e Tecnologie Informatiche

Via Bassini 15, 20133 Milano, Italy

carla@mi.imati.cnr.it

date	Lat	Lon	I_0	Number of felt reports	date	Lat	Lon	I_0	Number of felt reports
1570/11/17	44.820	11.630	VII-VIII	49	1894/11/16	38.280	15.870	VIII-IX	297
1627/07/30	41.730	15.350	X	48	1898/06/27	42.415	12.905	VII-VIII	140
1638/03/27	39.030	16.280	XI	205	1904/02/24	42.100	13.320	VIII-IX	36
1693/01/11	37.130	15.020	XI	179	1907/10/23	38.130	16.020	VIII-IX	266
1695/02/25	45.800	11.950	IX-X	79	1909/08/25	43.150	11.403	VII-VIII	158
1703/01/14	42.680	13.120	XI	185	1911/02/19	44.120	12.080	VII	129
1731/03/20	41.270	15.750	IX	40	1911/10/15	37.700	15.150	X	43
1740/03/06	44.124	10.590	VII	31	1916/08/16	43.970	12.670	VIII	236
1741/04/24	43.425	13.004	IX	135	1919/06/29	43.950	11.480	IX	260
1743/02/20	39.850	18.780	IX-X	64	1920/09/07	44.180	10.280	IX-X	577
1781/04/04	44.235	11.797	IX	74	1922/12/29	41.724	13.670	VII	99
1781/06/03	43.594	12.506	IX-X	143	1927/12/26	41.700	12.700	VII	34
1783/03/28	38.780	16.470	X	323	1928/03/27	46.372	12.975	VIII-IX	289
1802/05/12	45.420	9.850	VIII	60	1929/04/20	44.470	11.130	VII	622
1805/07/26	41.500	14.470	X	207	1930/07/23	41.050	15.370	X	498
1808/04/02	44.830	7.250	VIII	92	1930/10/30	43.659	13.331	IX	220
1818/02/20	37.600	15.130	IX	121	1933/09/26	42.050	14.180	VIII-IX	322
1818/02/23	43.920	8.034	VII-VIII	43	1943/10/03	42.935	13.639	VIII-IX	86
1828/10/09	44.820	9.050	VII-VIII	86	1958/06/24	42.340	13.477	VII	14
1836/04/25	39.570	16.730	IX	42	1962/08/21	41.130	14.970	IX	207
1846/08/14	43.531	10.500	VIII-IX	83	1967/10/31	37.870	14.420	VIII	59
1857/12/16	40.350	15.850	X-XI	311	1968/01/15	37.770	12.980	X	161
1873/06/29	46.150	12.380	IX-X	187	1971/02/06	42.442	11.846	VII-VIII	64
1874/12/06	41.650	13.830	VII-VIII	43	1971/07/15	44.820	10.350	VII-VIII	221
1875/12/06	41.689	15.677	VII-VIII	95	1975/01/16	38.120	15.650	VII-VIII	305
1887/02/23	43.920	8.070	IX	1366	1978/04/15	38.150	14.983	IX	316
1891/06/07	45.570	11.170	VIII-IX	308	1980/11/23	40.850	15.280	X	1161
1894/08/08	37.650	15.120	IX-X	40					

Table 1: Date, epicentral coordinates, epicentral intensity, number of felt reports of 55 strong earthquakes drawn from DBMI04 (Stucchi et alii, 2007)

1909/08/25	median	mean	3rd quartile
$\Delta I = 0$	9.050	11.580	10.193
$\Delta I = 1$	20.300	31.690	26.014
$\Delta I = 2$	41.635	45.780	38.380
$\Delta I = 3$	52.890	68.140	55.799
$\Delta I = 4$	70.150	88.140	74.647
$\Delta I = 5$	98.305	124.760	125.291

Table 2: Synthesis of the information contained in the macroseismic field of the 1909/08/25 earthquake of VII-VIII intensity: median, mean and 3rd quartile of each set of epicenter-site distances with the same ΔI.

class	predictive distrib.			binomial distrib.		
	scoring	odds	discrepancy	scoring	odds	discrepancy
$\mathcal{C}_A$	$1.452^{(**)}$	$0.177^{(**)}$	$0.667^{(*)}$	$1.513^{(*)}$	$0.295^{(*)}$	0.634
$\mathcal{C}_B$	1.508	0.293	0.769	1.542	0.348	$0.604^{(**)}$
$\mathcal{C}_C$	1.613	0.408	0.838	1.728	0.583	0.722

Table 3: Criteria of forward validation applied to the Colfiorito 1997 earthquake; * indicates the best result.
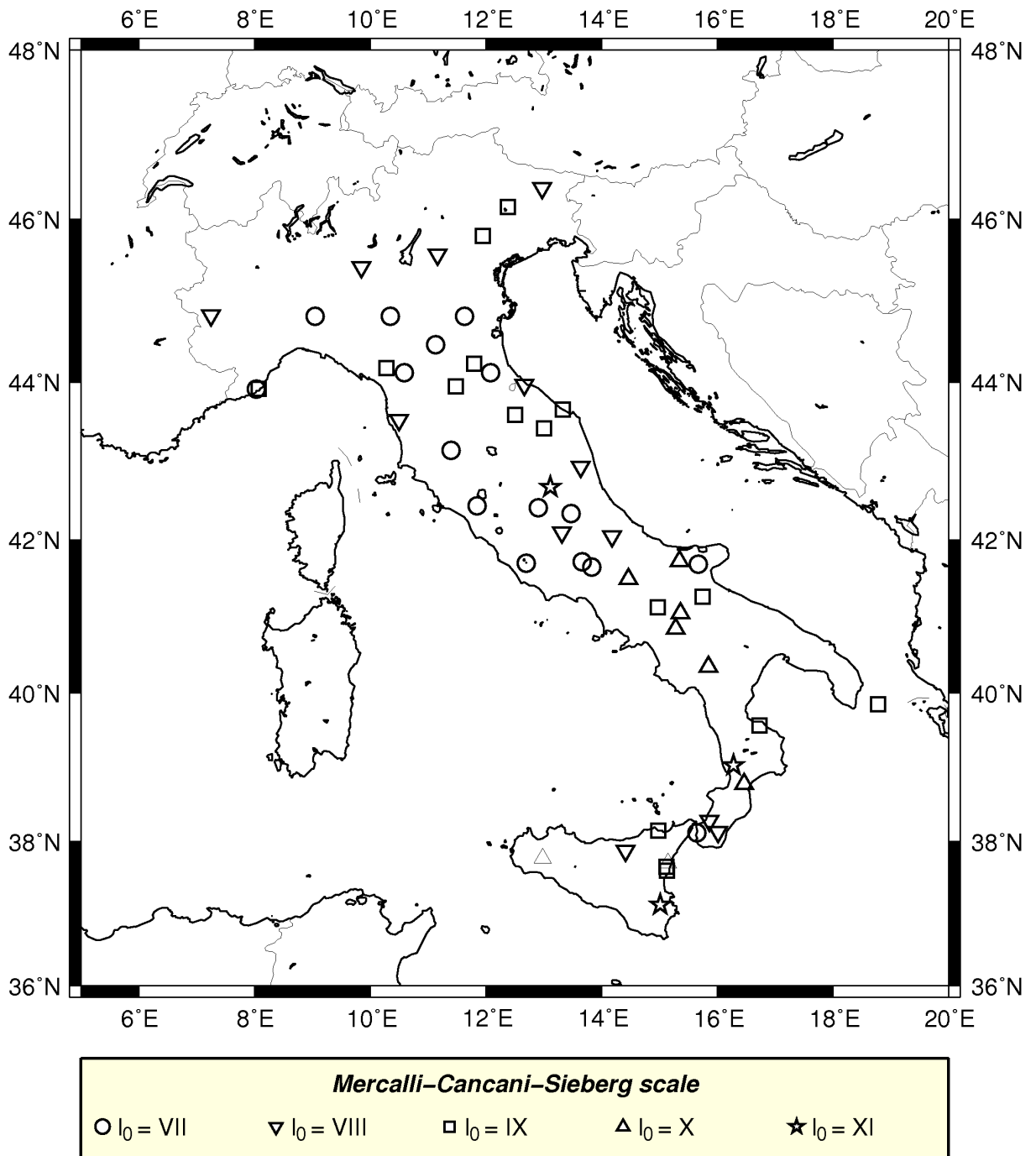
Figure 1: Spatial distribution of the epicenters of the 55 earthquakes constituting the data set.
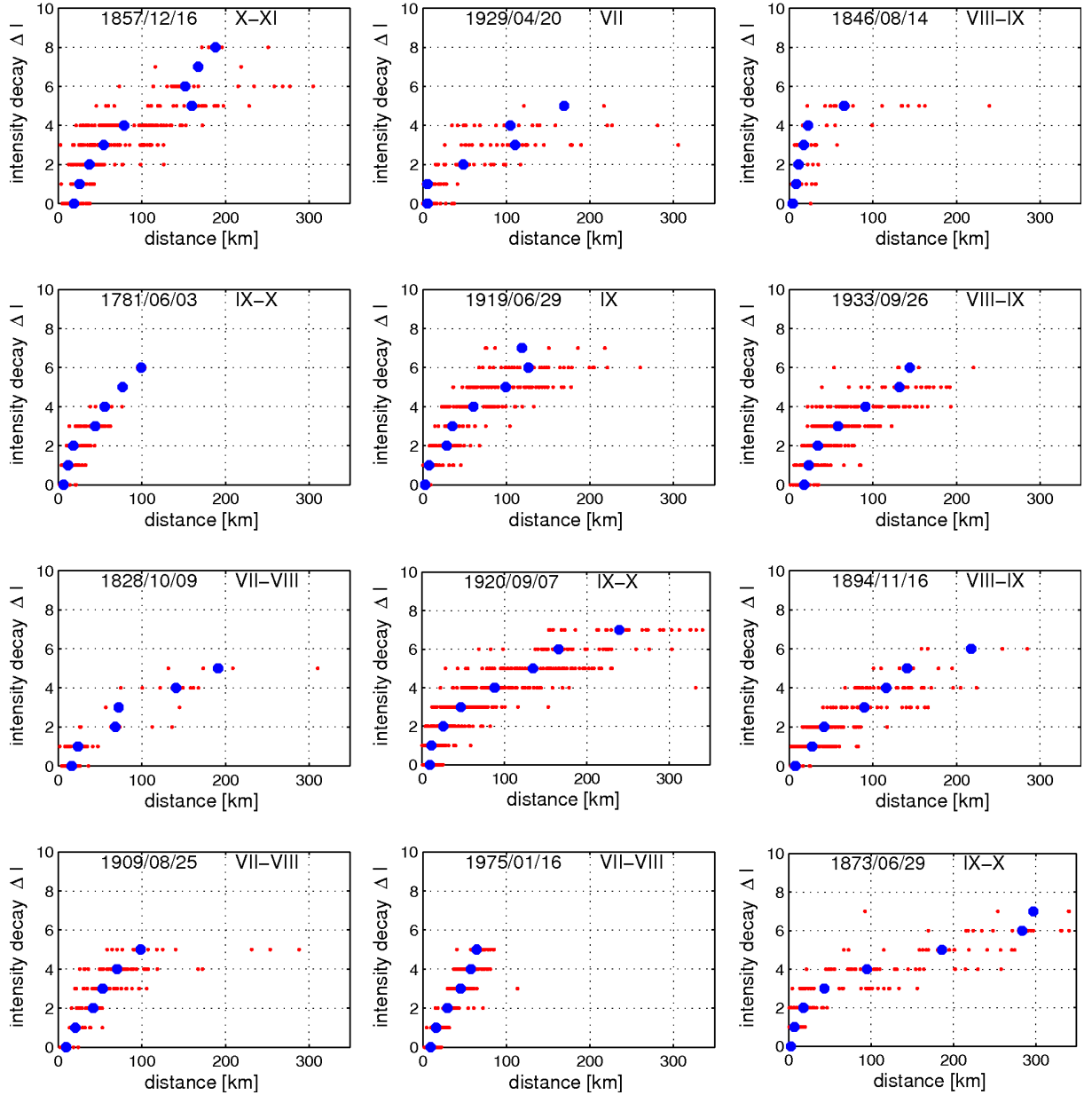
Figure 2: Intensity decay ΔI (red dots) *versus* epicentral distance for some of the 55 earthquakes examined. Setting $\Delta I = 0, 1, 2, \ldots, I_0 - 1$, the blue dot marks the median of the distances subsets. The title of each picture provides the date and macroseismic intensity of the earthquake concerned.
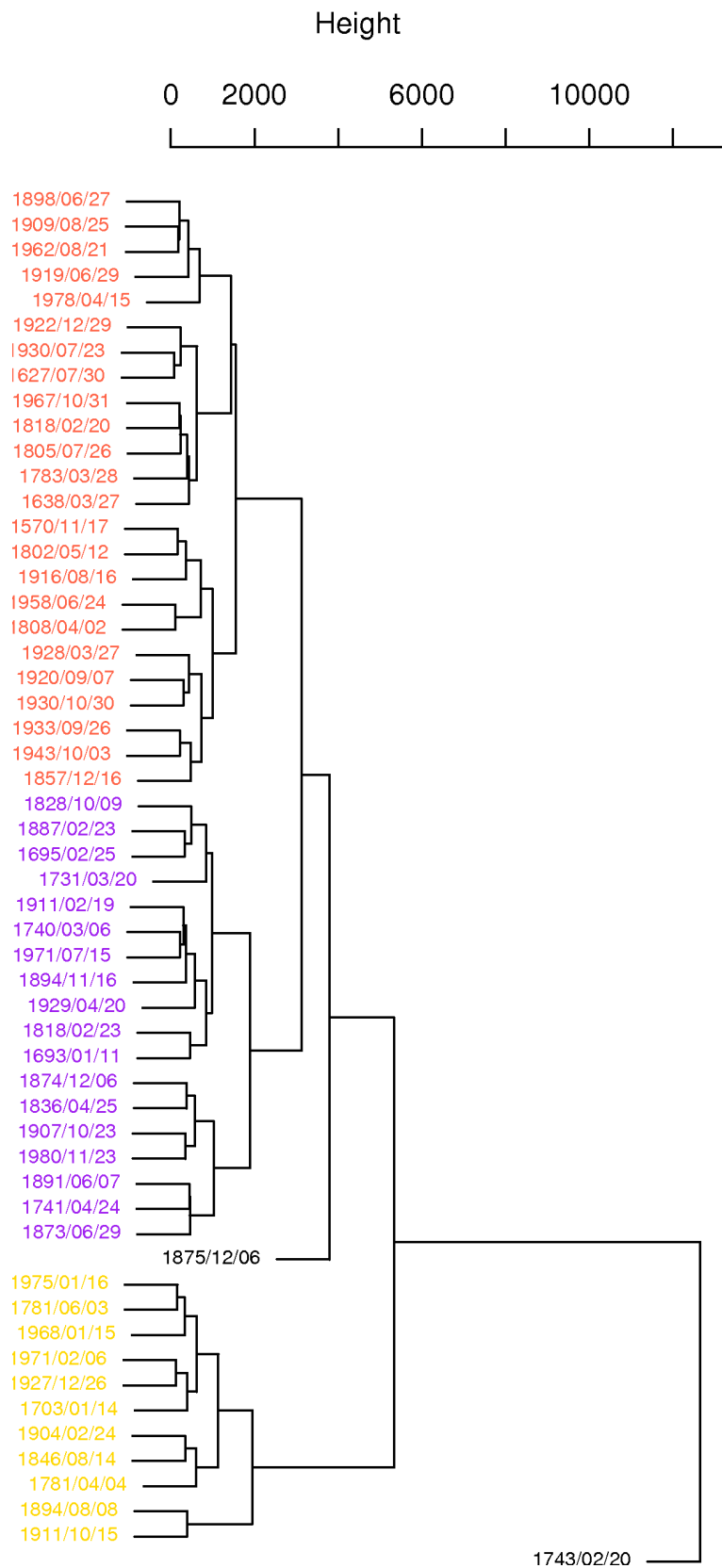
Figure 3: Cluster tree obtained by S-Plus software (2007) with the `Manhattan` metric and Ward's method. Three clusters are well-separated: the quickest (yellow), medium (red), and slowest (violet) attenuation trends. The 1875/12/06 and 1743/02/20 earthquakes have not been classified.

metric = Manhattan, method = Ward, k = 5

n = 55

5 clusters C_j

$j : n_j \mid ave_{i \in C_j} \; s_i$

1 : 24 | 0.34

2 : 18 | 0.17

3 : 11 | 0.28

4 : 1 | 0.00

5 : 1 | 0.00

Silhouette width s_i

metric = Manhattan, method = complete−linkage, k = 5

n = 55

5 clusters C_j

$j : n_j \mid ave_{i \in C_j} \; s_i$

1 : 39 | 0.31

2 : 12 | 0.36

3 : 1 | 0.00

4 : 1 | 0.00

5 : 2 | 0.68

Silhouette width s_i
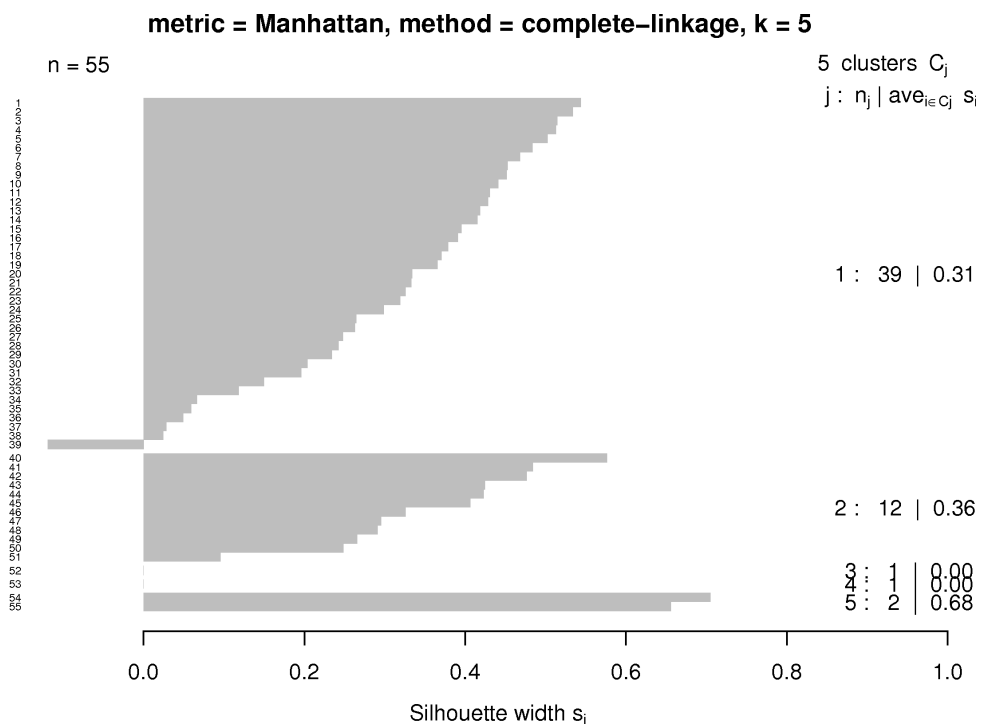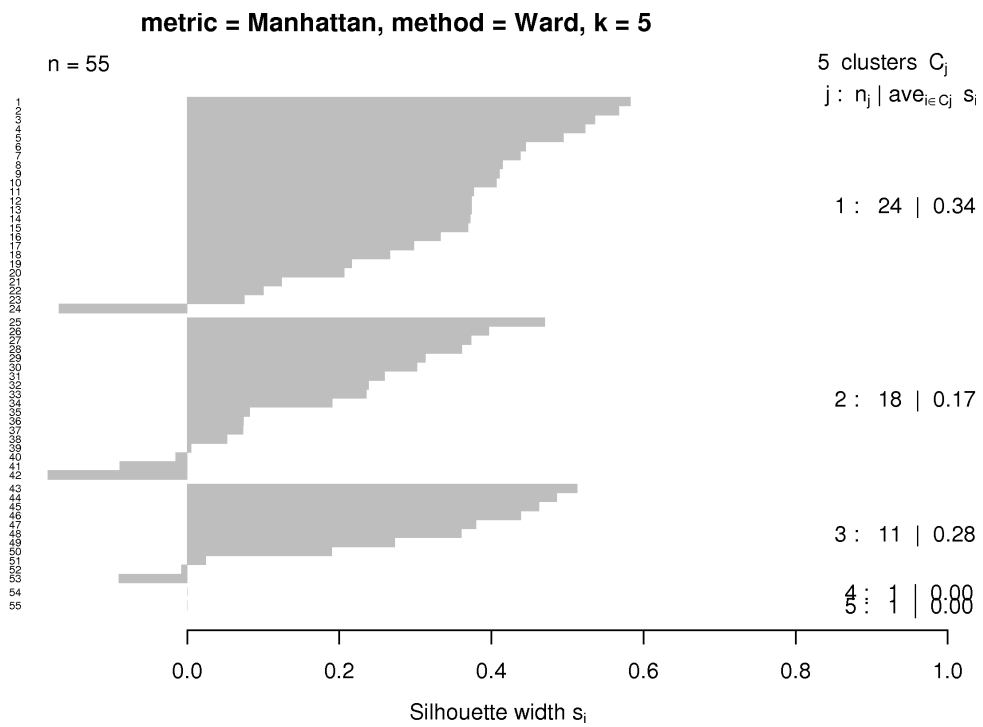
Figure 4: Silhouette plots generated by `Cutree`, a subroutine of the R free software (R, 2007) applying: `Manhattan` metric, $k = 5$ groups and Ward's method (top) and the complete-linkage method (bottom).
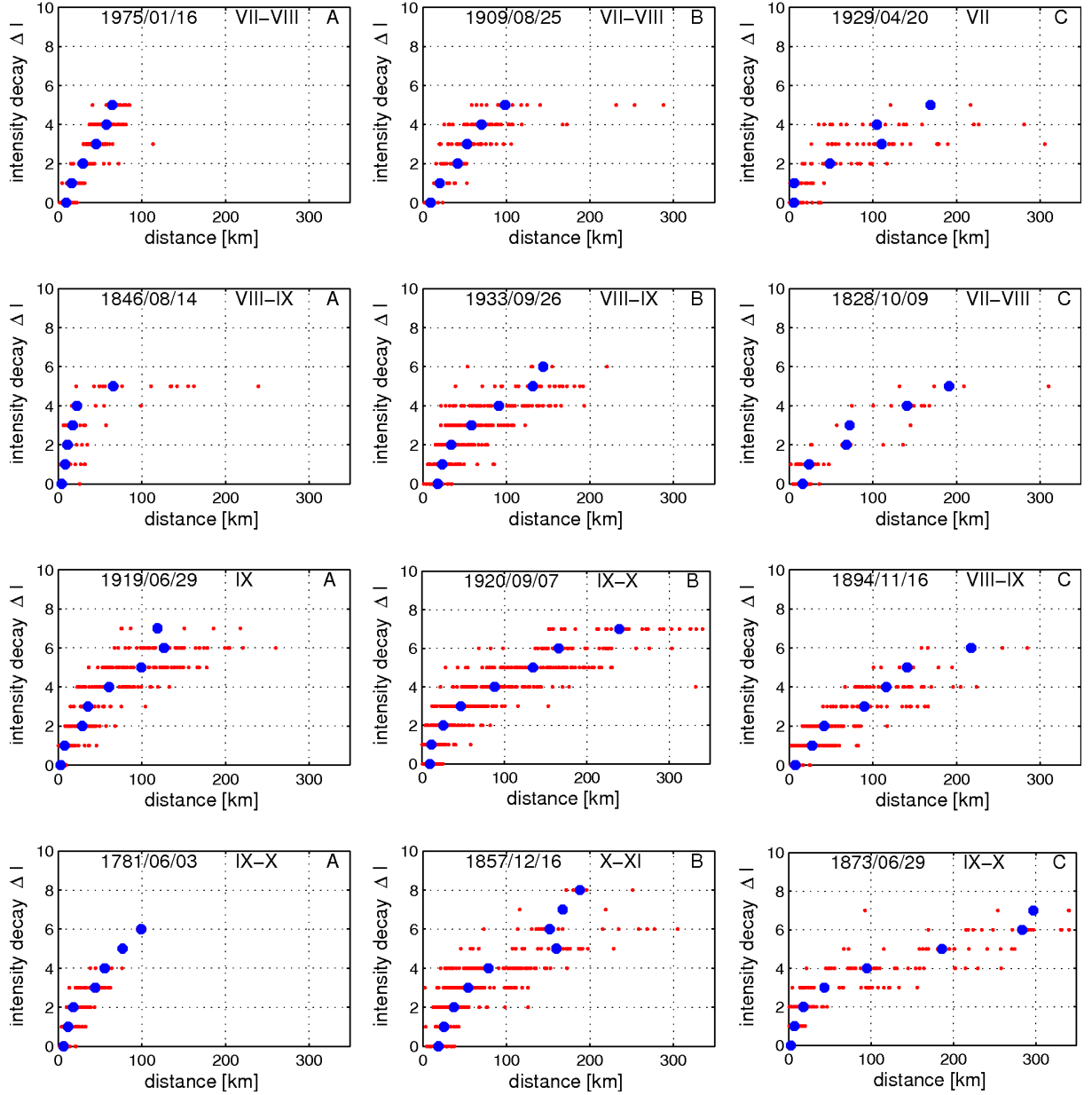
Figure 5: Intensity decay (red dots) *versus* epicentral distance for some of the 55 earthquakes examined. Setting $\Delta I = 0, 1, 2, \ldots, I_0 - 1$, the blue dot denotes the median of the distance subsets. The title of each diagram provides date, macroseismic intensity, and attenuation class of the earthquake concerned.
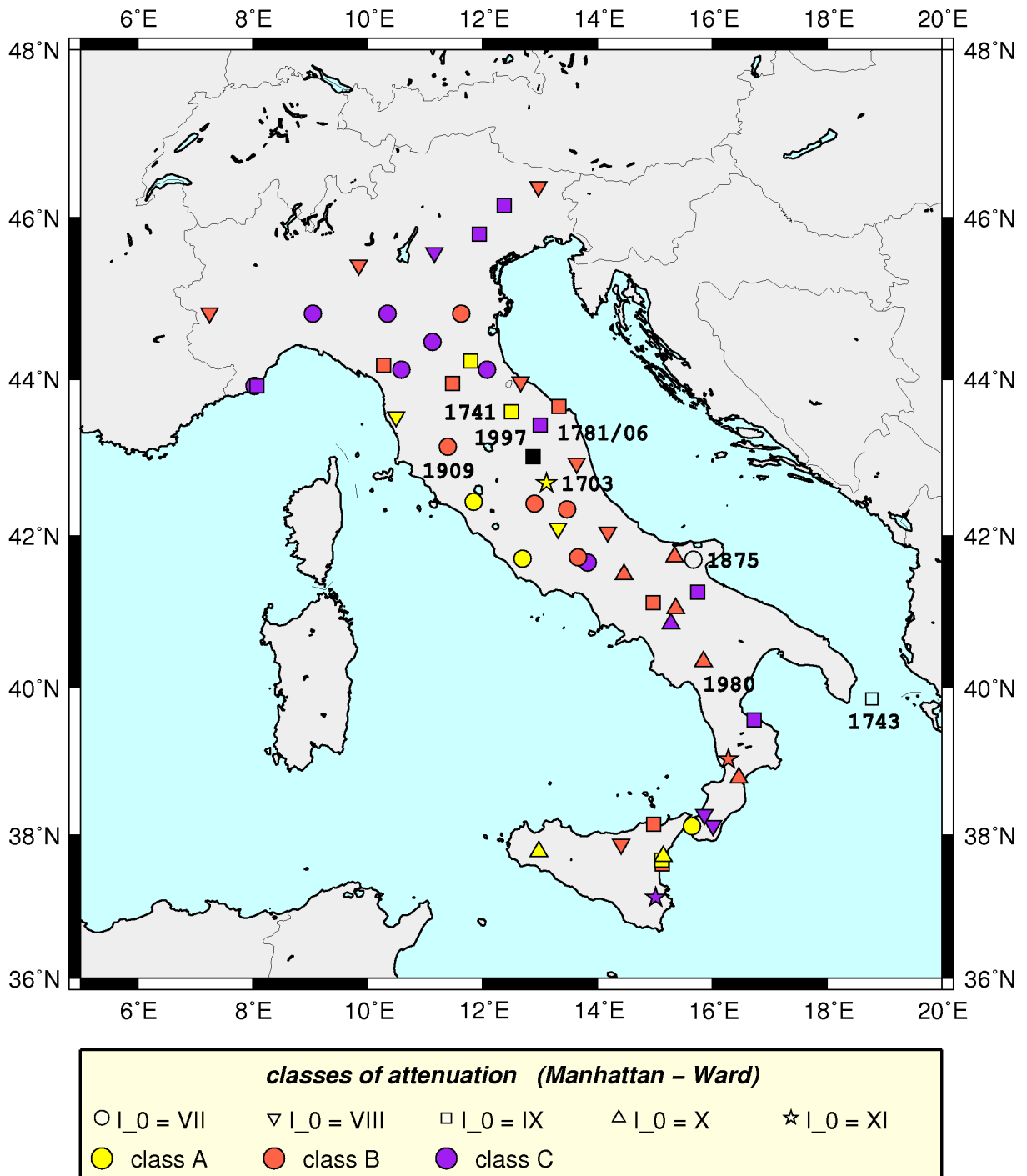
Figure 6: Classification of the data set in three attenuation trends: very steep (yellow), less steep (red), least steep (violet). The blank circle and square denote the unclassifiable earthquakes; the black square indicates the epicenter of the Colfiorito 1997 earthquake.
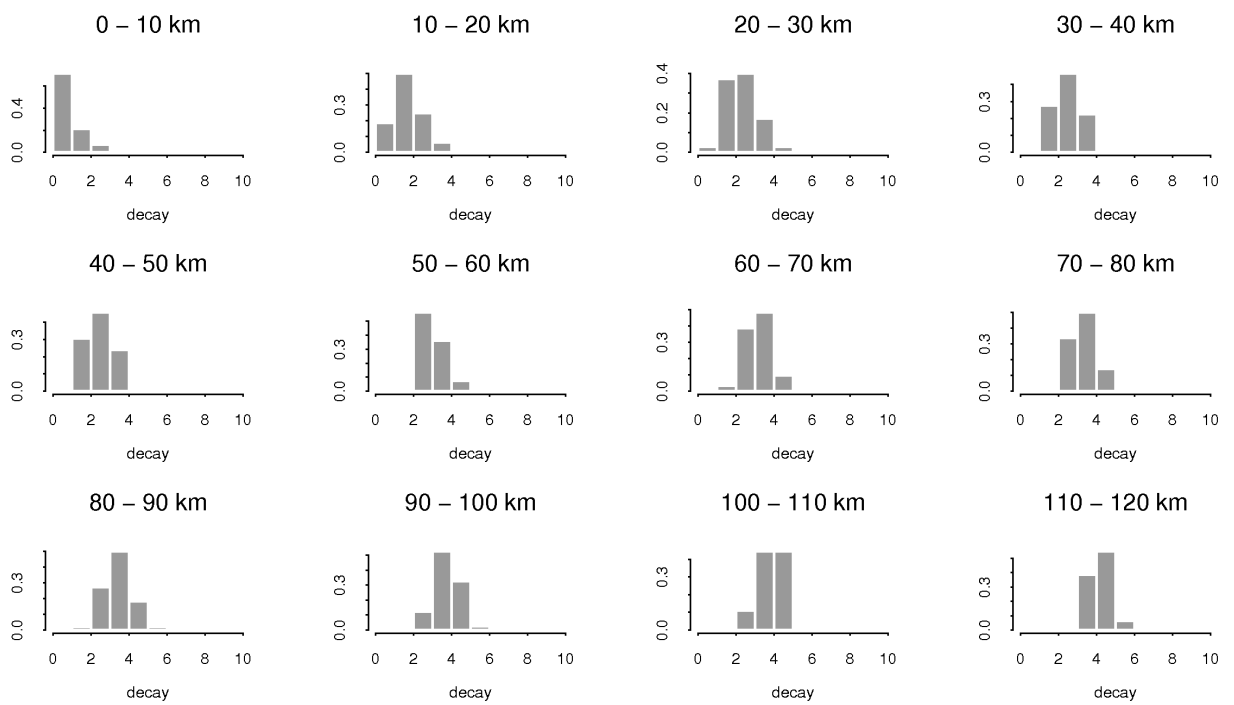
Figure 7: The 1980 Irpinia-Basilicata earthquake: relative frequencies of the intensity decay recorded in distance bins 10 km wide.
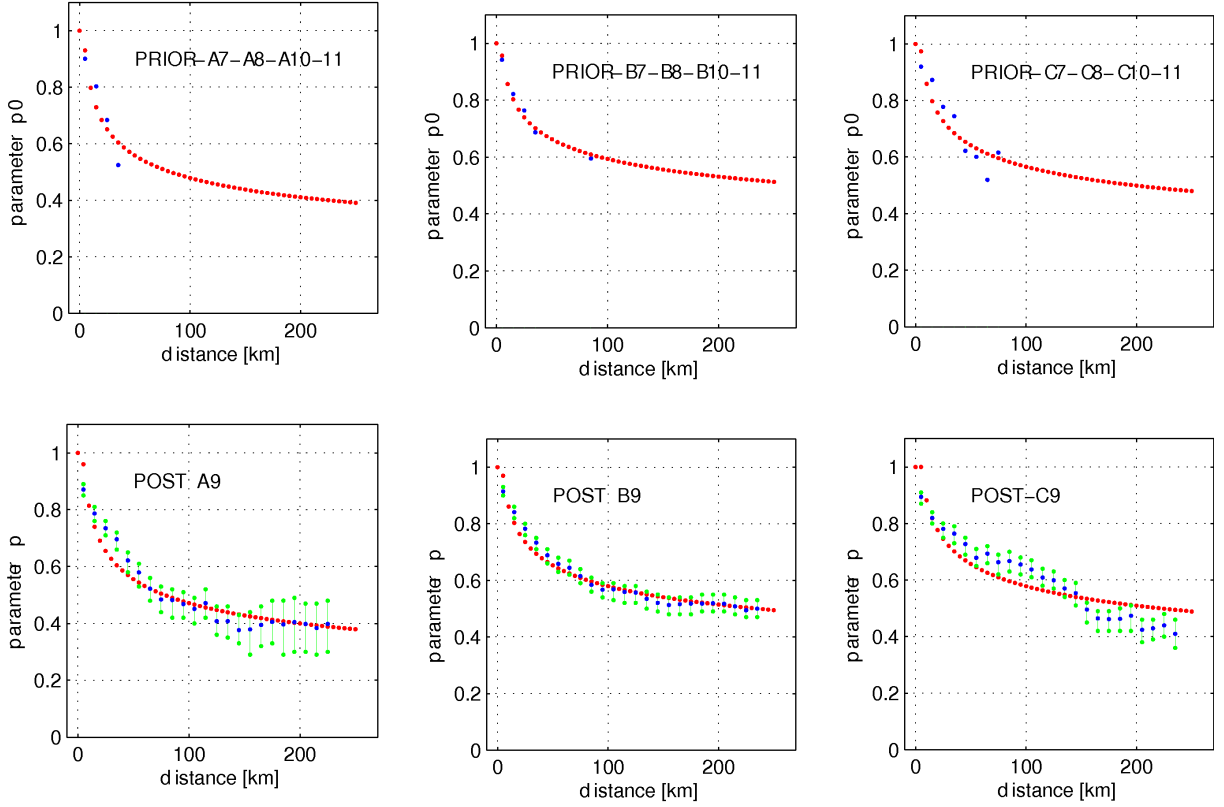
Figure 8: Prior and posterior p_j parameter (blue dots) of the binomial distribution of I_S conditioned on $I_0 = 9$ in the different classes $\mathcal{C}_A$, $\mathcal{C}_B$, $\mathcal{C}_C$, and at the jth bin, $j = 1, \ldots, 250$. The red dots indicate the *smoothing* inverse power functions, the green bars, the 90% confidence interval for each p_j.
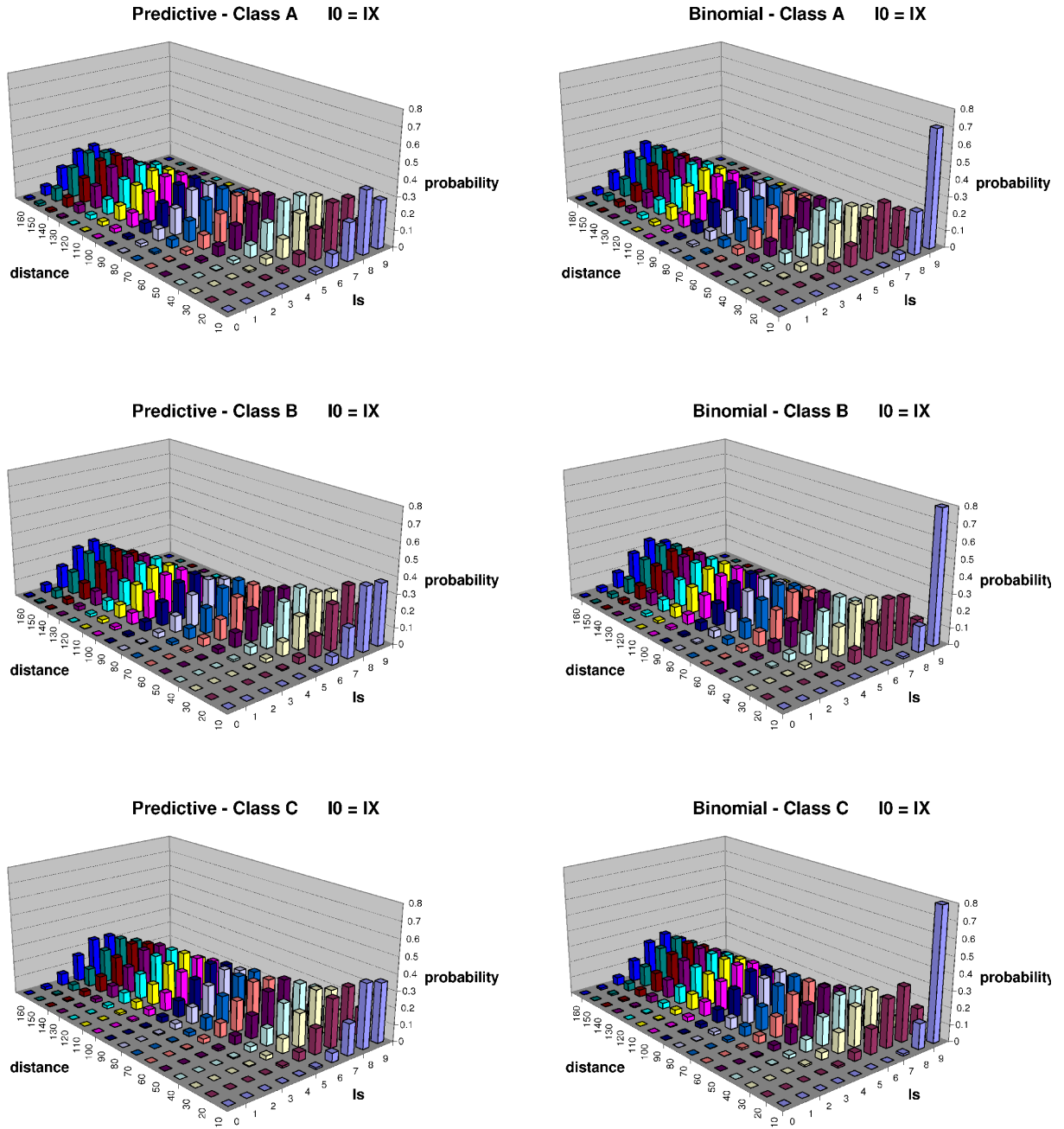
Figure 9: Predictive and binomial probability distributions in the jth bins, $j = 1, 2, \ldots, 160$.
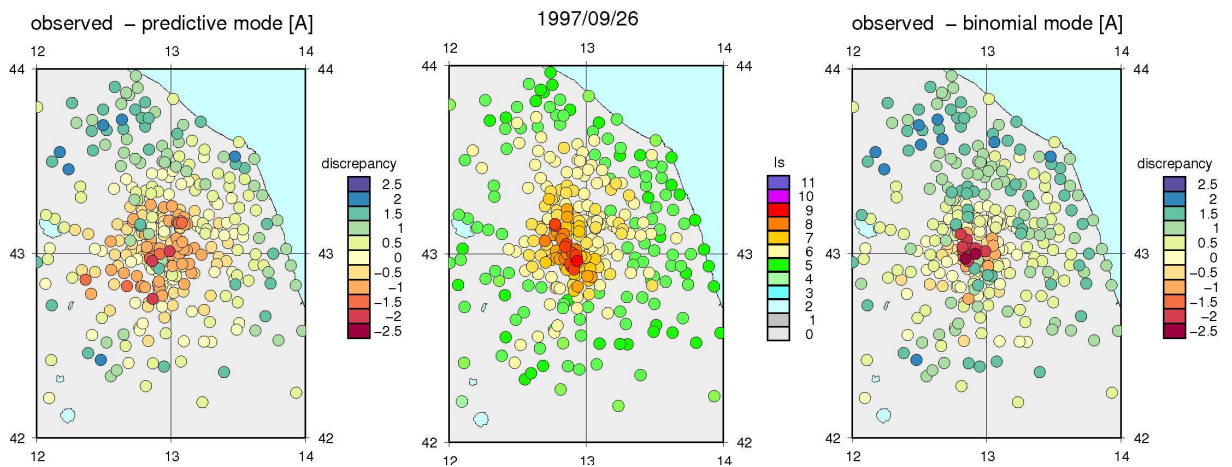
Figure 10: Macroseismic field of 1997/10/07 Colfiorito earthquake (midddle) and difference between the observed intensities and the best estimates (class A) produced by the predictive (left) and binomial (right) distribution.
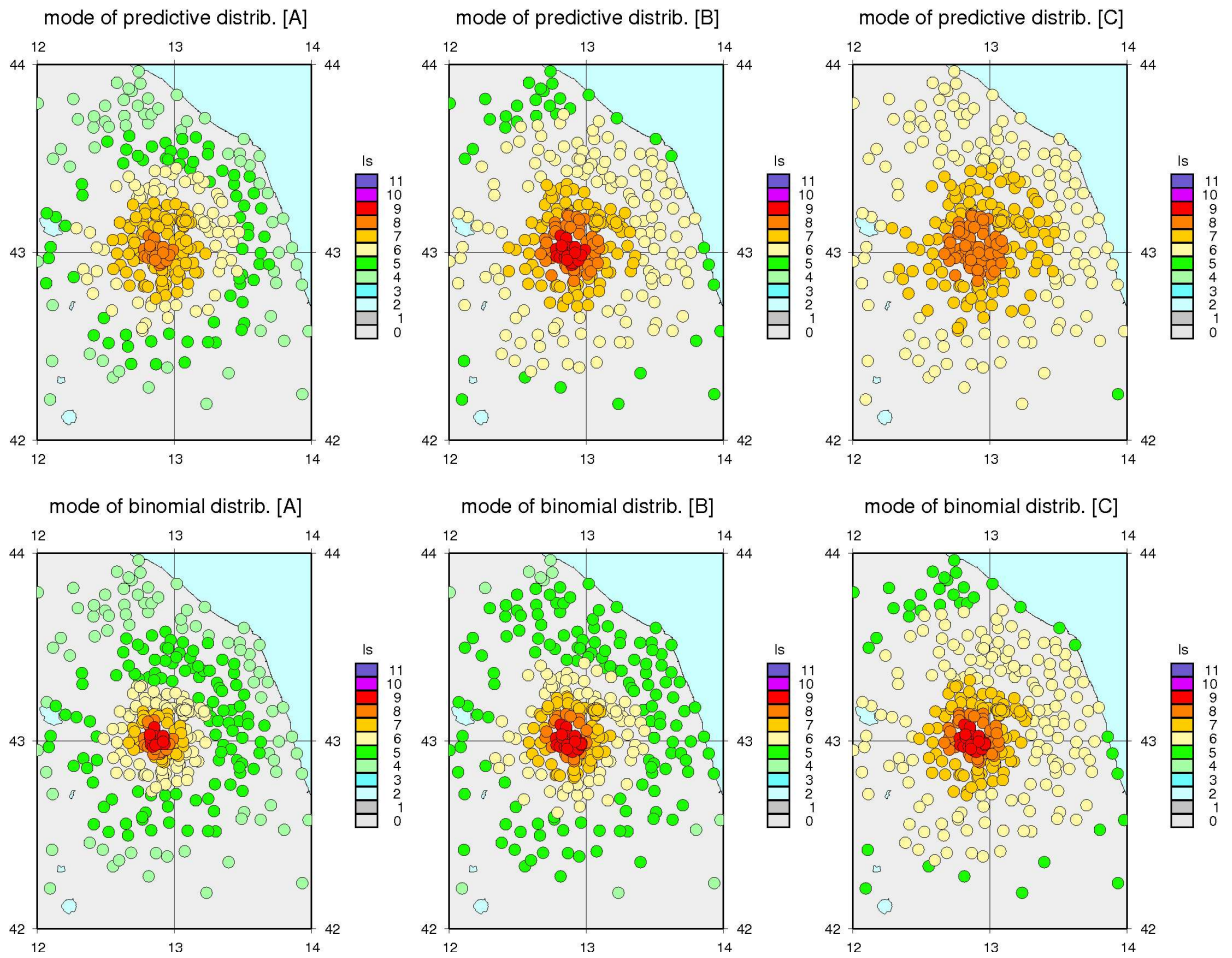
Figure 11: Estimate of the intensity at sites given by the mode of the predictive and binomial probability distributions.
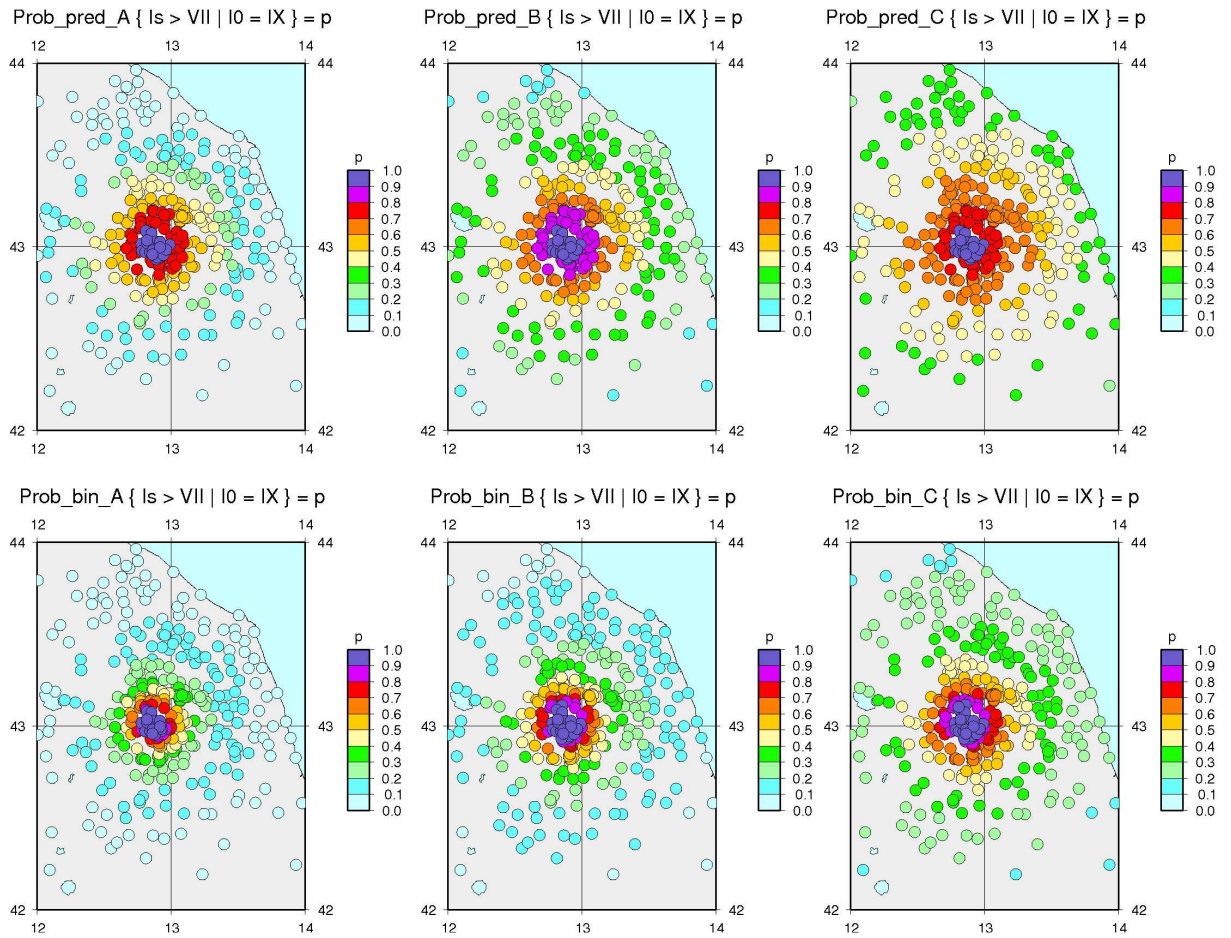
Figure 12: Forecast on Colfiorito macroseismic field: probability that the intensity at site exceeds the VII degree of the MCS scale according to predictive and binomial probability distributions.
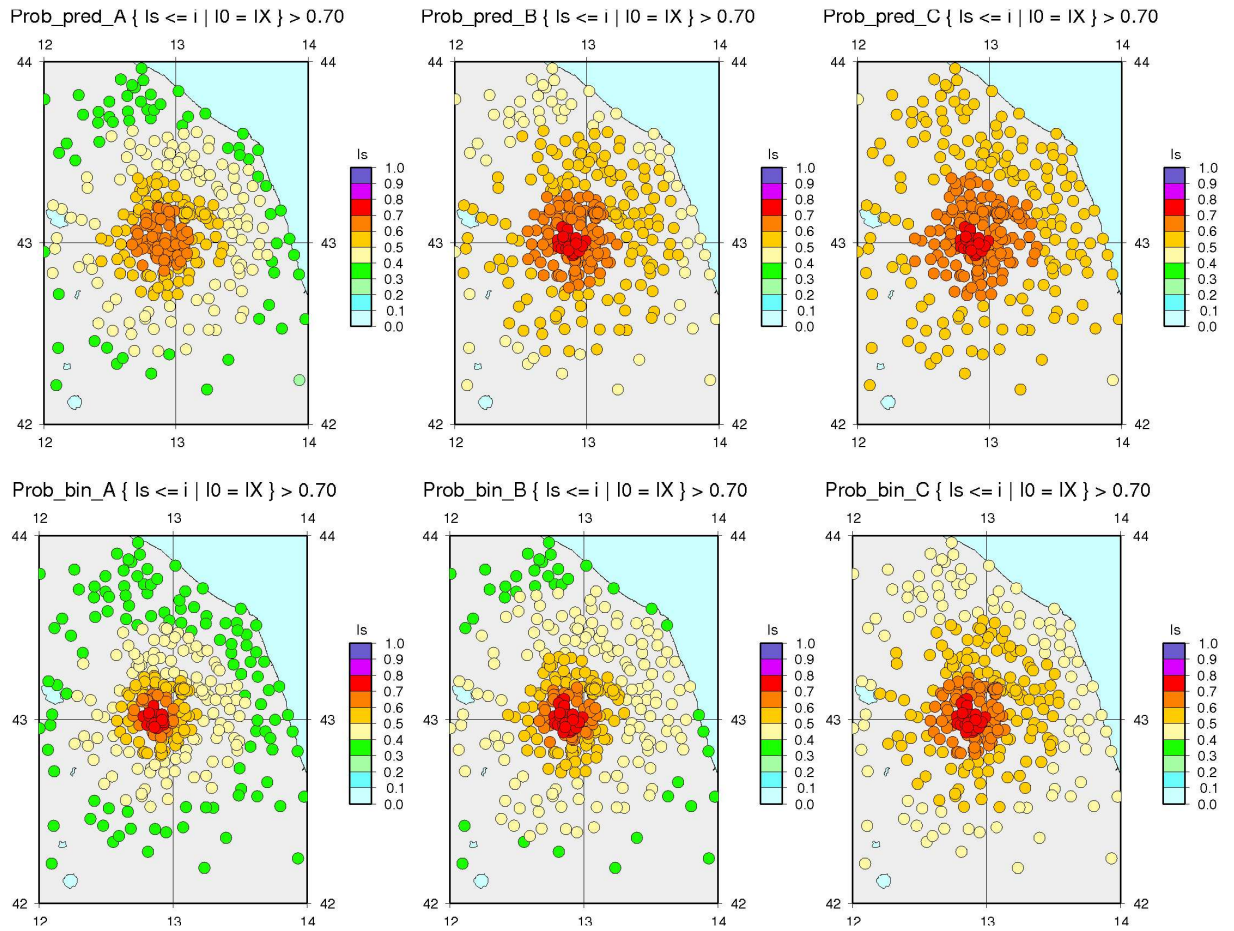
Figure 13: Forecast on Colfiorito macroseismic field: intensity at site not exceeded with a probability of at least 70% according to predictive and binomial probability distributions.